Nuclear Instruments and Methods in Physics Research A303 (1991) 277–284
North-Holland

Design and performance of a straw tube drift chamber

S.H. Oh, D.K. Wesson, J. Cooke, A.T. Goshaw, W.J. Robertson and W.D. Walker
Department of Physics, Duke University, Durham, NC 27706, USA

Received 19 November 1990

The design and performance of the straw drift chambers used in E735 is reported. The chambers are constructed from 2.5 cm radius aluminized mylar straw tubes with wall thickness less than 0.2 mm. Also, presented are the results of tests with 2 mm radius straw tubes. The small tube has a direct detector application at the Superconducting Super Collider.

1. Introduction

Drift chambers are now used in almost every high energy physics experiment. There are many different designs of drift chambers and one of them uses straw tubes as detector elements [1]. In this article, we report the design, construction, and performance of large straw tube drift chambers used in the spectrometer arm of E735 at the Fermilab collider. E735 is an experiment to study low transverse momentum particles to search for a phase transition of hadron gas to quark–gluon plasma from the highest center of mass energy $\bar{p}p$ interactions [2]. We also present preliminary results of a study done with 2 mm radius tubes which have a direct detector application at the Superconducting Super Collider (SSC).

Using straw tubes has several advantages. First, since the cells are isolated from one another, cross talk is minimized. If a sense wire is broken, then the channel can be easily removed without turning off all channels. Second, straw tubes can be pressurized for better resolution, and for mechanical rigidity. Third, the resolution of tracks is independent of a particle's incident angle, so one does not have to incorporate angular correction factors when the drift distance is calculated from the drift time, as with typical drift chambers. This was the main reason we chose straw drift chambers since tracks in the spectrometer arm have large slopes.

This article is organized as follows. In section 2, we discuss the design and construction of chambers, and in section 3, testing and performance of the chambers are discussed. In section 4 we describe a method to measure the drift velocity and resolution. Section 5 includes the track reconstruction in the chambers, and section 6 contains a study done with 2 mm radius tubes, which may have a detector application for the Superconducting Super Collider.

2. Design and construction of chambers

The basic ingredient of the chamber is a 2.5 cm radius tube made of aluminized mylar. The wall of the tube consists of 0.018 mm of aluminum, 0.075 mm of paper and 0.075 mm of mylar, a thickness of about 0.04% of a radiation length. The tubes were wound by Stone Industrial [3] with length of about 110 cm. The tubes are strong enough to support about 10 kg of weight placed on one end, and an internal pressure of at least 3 atm.

The tubes are positioned between two aluminum plates as shown in fig. 1. Two aluminum plates on both the top and the bottom provide protection for the tube ends, feed-throughs and electronics. The size of the holes and the distance between holes were milled to be better than 0.1 mm. There are about 60 to 100 holes in each chamber. The holes in each chamber are in two staggered rows. After the holes were made, the center of each hole was measured with respect to a survey point to determine the exact position of the sense wire.

As shown in fig. 2, each tube is connected to the plates by means of aluminum end-pieces. A hose clamp is used to ensure the mechanical and electrical connection between the aluminum end-piece and the tube. Each aluminum piece is grounded to the frame by a ground cable. An end-piece made of delrin and a feed-through are inserted into the aluminum end-piece. 100 μm diameter gold plated Cu–Be wire is strung between feed-throughs under 250 g of tension. The elastic limit of the wire is about 1000 g. Cu–Be wire is used because its thermal expansion coefficient is close to that of the aluminum frame. A larger diameter wire is chosen to provide a higher electric field near the outer wall of the tube. The drift velocity saturates if the electric field is high enough.

Gas leakage, especially around the ends of the tubes,

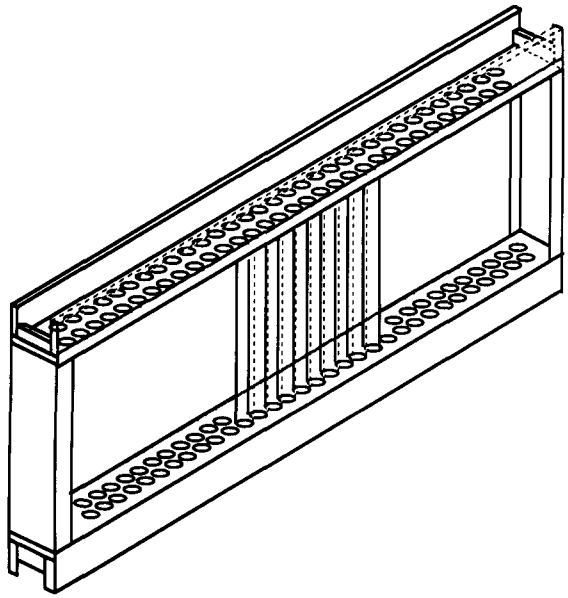

Fig. 1. The aluminum frame structure of a straw drift tube chamber for E735. A few tubes between the two aluminum plates are also shown.

was a major problem during construction. The gas seal is accomplished by pouring low viscosity RTV-615 around the tubes. RTV-112 is used to provide the gas seal around the feed-throughs and around the gas tubing.

Gas is provided by 0.6 cm diameter plastic tubing at the top of the aluminum end-piece. 16 tubes are connected in series and an independent gas line is provided for each group of 16. This is to minimize contamination to other tubes in a chamber in case a tube develops a leak. When data is being taken, each chamber receives gas at a rate of about 1 ft^3/h.

The output from the sense wire is connected to an amplifier-discriminator through a 0.001 μF capacitor. The amplifier–discriminators are mounted on the top part of the frames of the chambers near the ends of the tubes. The amplifier–discriminator is designed using MC10116 and its performance is quite comparable with LeCroy 2735DC whose minimum threshold is 2 μA. 130 ft of twisted pair ribbon cables connect the output of the amplifier–discriminator to LeCroy TDCs. We have used 4299B with 1 ns time resolution.

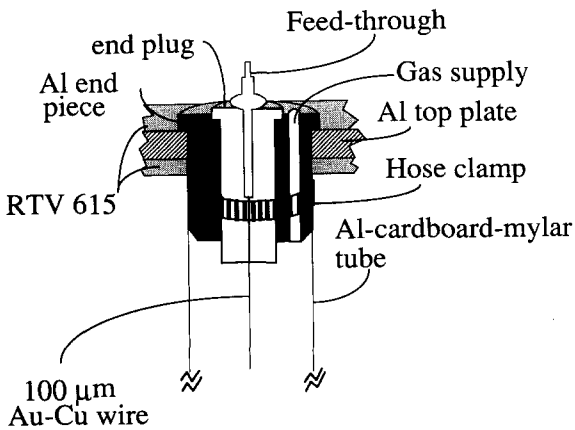

Fig. 2. A detailed view of a tube end including end pieces.

There are seven chambers with two planes of tubes in each chamber. The size varies from 75 cm (height) × 220 cm (length) to 110 cm × 340 cm. Four out of seven chambers have tubes positioned vertically to measure the horizontal position of tracks. The strong component of the magnetic field is along the vertical direction. The tubes in the other three chambers are slanted by 4° for stereo reconstruction. When in place, chambers with slanted tubes alternate between chambers with vertical tubes. There are about 700 channels in the detector.

3. Testing and performance of chambers

In order to find the operating voltage for the chambers, the singles rate as a function of voltage was studied. Fig. 3 shows a typical plateau taken with cosmic rays, and ^{137}Cs source with Ar–ethane (50%–50% mixture). The operating voltage is selected at the end of the plateau curve as shown in the figure.

After chambers were constructed, we measured the resolution by using cosmic rays. A chamber is sandwiched between two scintillators. A trigger is generated from the coincidence signal from the two scintillators and used to start the TDC. The measured time is converted to distance from the sense wire. For the

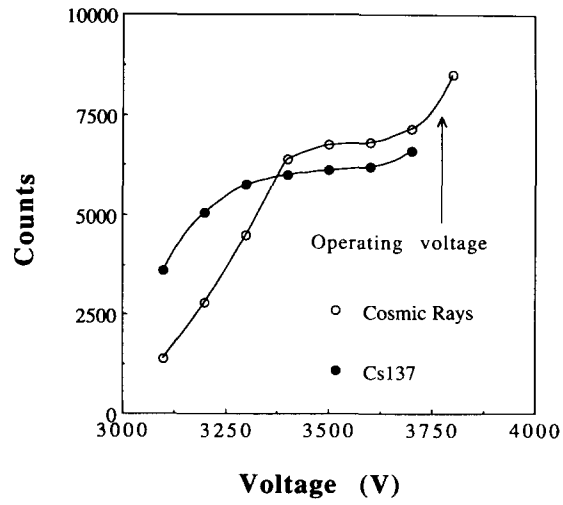

Fig. 3. Two plateau curves obtained using cosmic rays and ^{137}Cs. The gas used is Ar–ethane (50%–50% mixture).

conversion, the drift time as a function of distance is measured (section 4) and plotted. This curve was fitted with a polynomial and used to convert the measured time to distance. Sometimes it was necessary to divide the data into two regions to get a good overall fit. After the conversion of time to distance, tracks were reconstructed (section 5) and the residual was calculated.

We have tried two different gas mixtures, Ar–ethane (50%–50%) and P10 (Ar–methane, 90%–10%). The Ar–ethane mixture produced slightly better resolution than Ar–methane mixture. Fig. 4 shows the residuals for the two gases, and the σ is less than 200 μm. The residual is calculated from tracks with more than 6 hits.

An earlier study [4] showed that the radiation level from the accelerator at the chamber position was expected to be high. Therefore a radiation test was performed on a prototype consisting of a single tube. The tube was exposed to an intense source (^{90}Sr) such that the sense wire drew about 1 μA/cm. This corresponds to about 0.09 C cm^{-1} d^{-1}. We used the Ar–ethane (50%–50%) mixture for the test because of the higher hydrocarbon content. Hydrocarbon is a known aging agent. The exposure lasted for four months with periodic checks made of the current draw, single count and the shape of plateau. The results of the current draw and the single count as a function of integrated charge/cm on the sense wire is shown in fig. 5. They remained constant during the period. After the test, the tube was opened and examined for radiation damage. No signs of whisker growth or other deterioration were found. It was reported that some chambers using the same gas became inoperative after much less dosage [5]. We believe that this is due to the lower electric field at the cathode and a much larger cathode area.

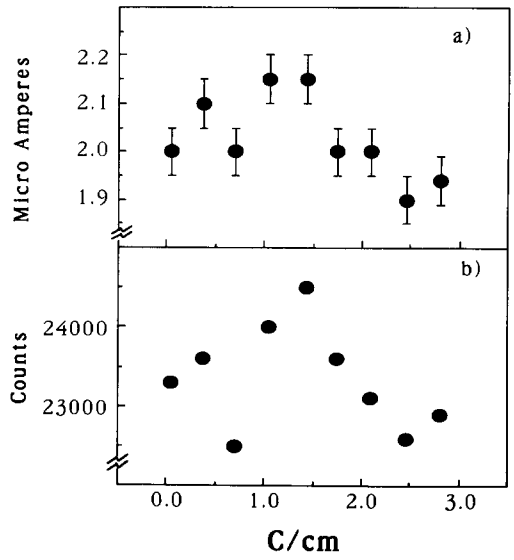

Fig. 5. Results of an aging test using ^{90}Sr source. (a) Shows the current draw by the sense wire as a function of total charge deposited on the sense wire. (b) Shows the single count as a function of total deposited charge.

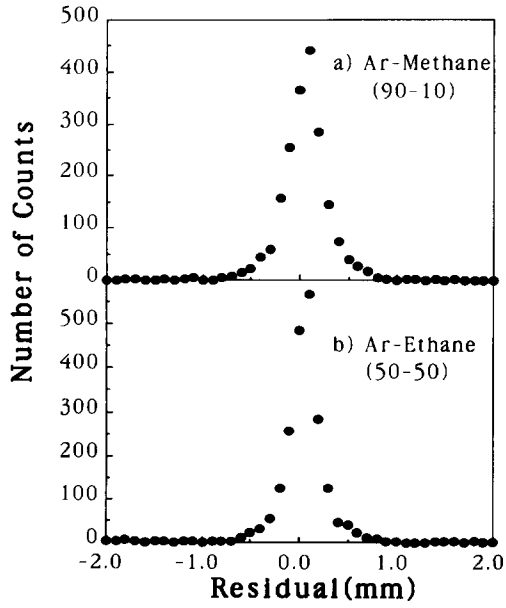

Fig. 4. The residual obtained using cosmic rays for two different gases. The sigma is less than 200 μm for both gases.

4. Drift velocity measurement

We have used a simple method to measure the relationship between the drift time and the distance from the sense wire. A 1 mCi ^{90}Sr source is placed in front of a slit followed by a chamber and another slit as shown in fig. 6. The two slits (1 mm wide and 1 cm in height) determine the beam position. A scintillator is placed behind the second slit and used to start a TDC and the signal from the tube is used to stop the TDC. Since the energy of electrons from the ^{90}Sr source is low, we did not use the coincidence of two scintillators. We used one small scintillator large enough to cover the slit to reduce the random background start. This method provides a fast way to measure the drift velocity and resolution of different gases under operating conditions as shown below.

The time distribution for a given slit position is plotted and fitted with a Gaussian to determine the mean time and σ. The mean time and σ are plotted as a function of the slit position. In fig. 7 the mean time is plotted as a function of distance for methane. The position of the sense wire is the intersection point between two curves which fit the data points in the left and right side of the sense wire. By differentiating the fitted curve, the drift velocity can be calculated as a

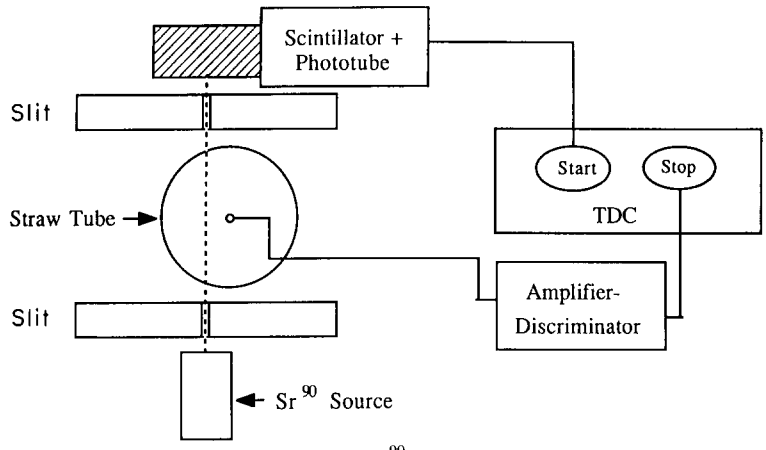

Fig. 6. Schematic to measure drift velocity and dispersion using a ^{90}Sr source. The size of the slit is 1 mm (width) by 1 cm (height). See text for details.

function of the distance from the sense wire or the electric field since the electric field is easily calculable for the cylindrical geometry. In fig. 8, the measured drift velocity as a function of electric field is plotted for several gases. Fig. 8a shows the electron drift velocity for Ar–ethane (50%–50%) and P10 (90% Ar–10% methane). Fig. 8b shows the same for pure methane and methane with 5% ethyl-alcohol. This mixture is tried because mixing alcohols increases the lifetime of chambers. Mixing alcohol changes the characteristics of the drift velocity as a function of the electric field.

In fig. 9, the drift velocity using mixtures of CF_4 and CH_4 is presented. The mixtures are tested because of a possible application to an SSC detector. For an SSC drift chamber, gas with fast electron drift velocity (larger than 100 μm/ns) is desirable since the time between bunches is 16 ns (see section 4). As seen from the figure, pure CF_4 as well as the mixtures of CF_4 and CH_4 have drift velocities larger than 100 μm/ns. Although not plotted, some of our data points are compared with the existing data [6] and they are in fair agreement.

The σ of the time distribution is related to the resolution as a function of drift distance. We convert the σ, measured in time to distance using the time to distance conversion plot, i.e., $t \pm \sigma_t$, in time to $d \pm \sigma_d$ in distance. We point out that the σ_d does not measure the absolute resolution directly because of the slit size and the multiple Coulomb scattering of electrons. However σ_d provides a good way to compare the relative resolution as a function of the drift distance between different gases.

In fig. 10a the σ_d (dispersion) is plotted as a function of drift distance. For P10 and Ar–ethane, the dispersion is fairly constant as a function of distance. In fig. 10b, the same is plotted for methane and methane with 5% ethanol. It is interesting that the dispersion rises steeply

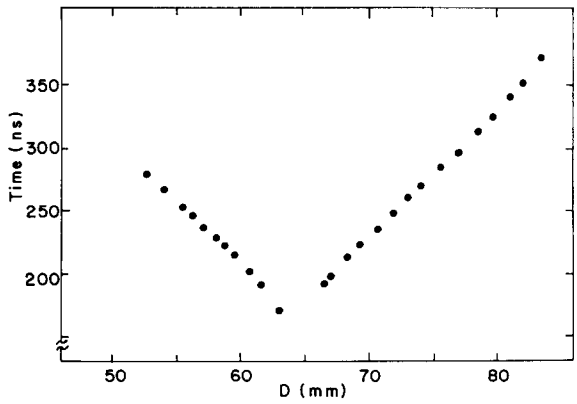

Fig. 7. A typical mean drift time plotted as a function of distance. The sense wire is at the symmetry axis. The data is obtained with CH_4.

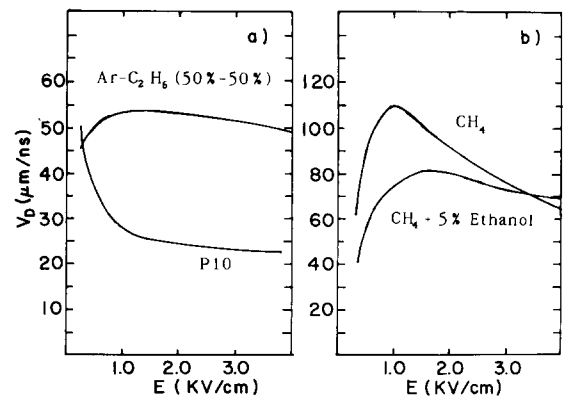

Fig. 8. Drift velocity as a function of electric field as measured using the setup in fig. 6 for P10, Ar–ethane (50%–50%), CH_4, and CH_4 + 5% ethanol.

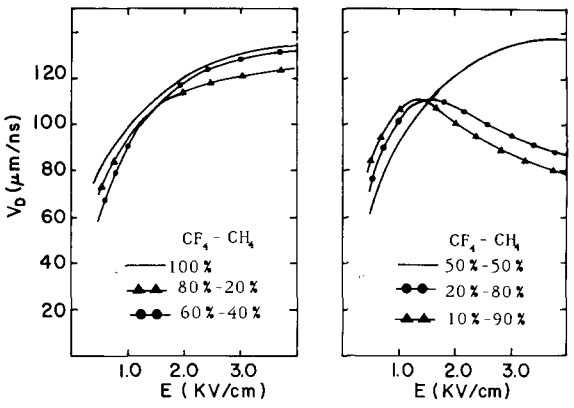

Fig. 9. Same as fig. 8, but with different mixtures of CF_4 and CH_4.

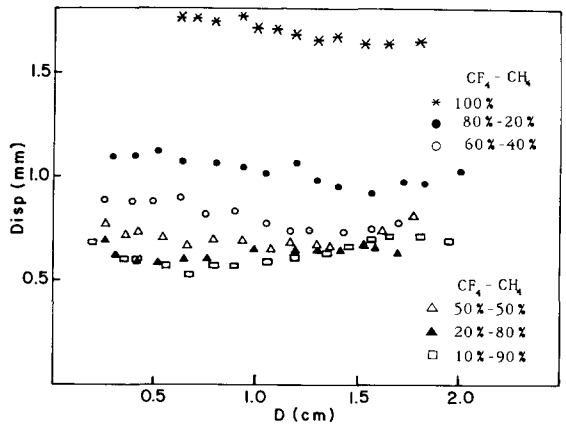

Fig. 11. Dispersion as a function of drift distance for different mixtures of CF_4 and CH_4.

at a certain distance from the sense wire when the alcohol is mixed. This may be due to the electron attachment to alcohol molecules. We have tried several mixtures of different gases with different kind of alcohols, and we found that mixing alcohol always increases the dispersion at a large distance (~ 1 cm from the sense wire).

In fig. 11, the dispersion is plotted for the mixtures of CF_4 and CH_4 as a function of distance. It was shown earlier that these mixtures produced fast electron drift velocity as required for an SSC detector application. Fig. 11 shows that CF_4 alone is not a suitable gas for a drift chamber due to a large dispersion. As will be shown later, pure CF_4 not only results in a large dispersion, but also produces a long tail in the time distribution. The dispersion is reduced when CH_4 is mixed. The reduction increases as the fraction of CH_4 increases.

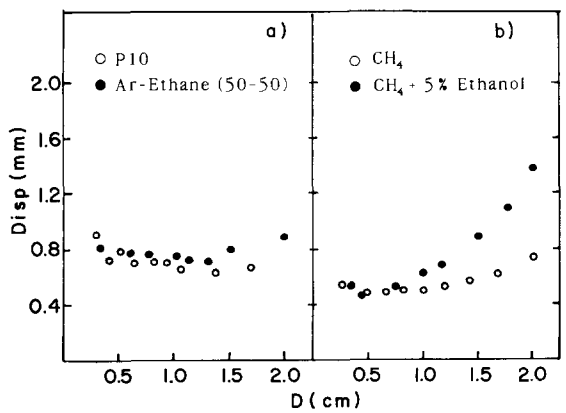

Fig. 10. Dispersion as a function of drift distance from the sense wire for several different gases; P10, Ar–ethane (50%–50%), CH_4 and CH_4 + 5% ethanol.

Mixing other hydrocarbon gases, such as ethane produces the same effect. It seems to us that a mixture with more than 50% of CH_4 may be acceptable in terms of dispersion.

In fig. 12, the converted time distribution (to distance) is plotted when the slit is about 2 mm away from the sense wire for different mixtures of CF_4 and CH_4. As pointed out earlier, pure CF_4 produced a long tail.

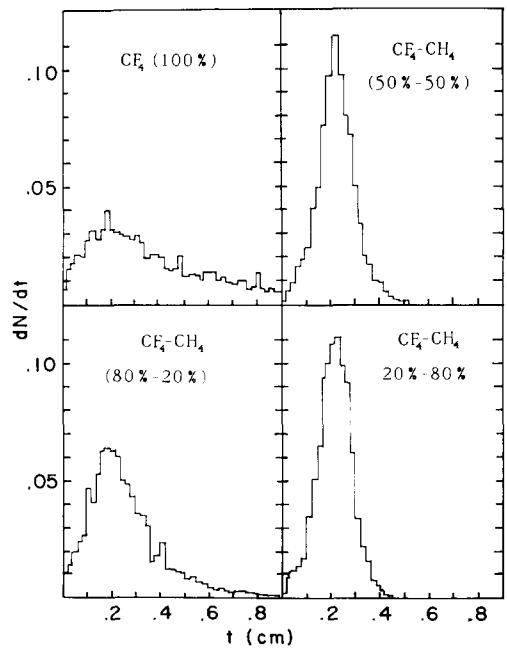

Fig. 12. Converted time (to distance) distribution when the slit is about 2 mm away from the sense wire for different mixtures of CF_4 and CH_4. The width of the slit is 1 mm.

The dispersion and the tail get smaller as the CH_4 content increases.

5. Track reconstruction

Fig. 13 shows some tracks passing through the chambers. Since a drift time represents the distance from the sense wire, a hit is represented by a circle around the sense wire. Tracks are reconstructed in the chambers with vertical tubes and then the chambers with slanted tubes are used for the stereo reconstruction.

The first step to reconstruct a track is to calculate the four possible tangential lines between two circles as shown in fig. 14. The two circles are chosen in the furthest chamber from the interaction region to avoid any field from the analysis magnet. The magnetic field strength is a Gaussian with maximum strength of 3 kG. The field strength drops to about 700 G at the first chamber (20 cm from the center) and to about 10 G at the last chamber location (100 cm from the center of the magnet).

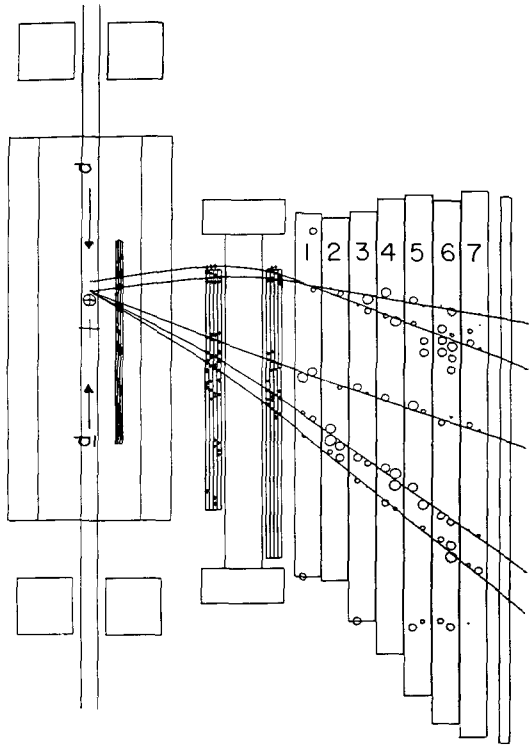

Fig. 13. Tracks passing through the E735 spectrometer arm. E735 is one of the collider experiments at Fermilab. Hits in the straw chambers are represented by a circle with a radius corresponding the converted drift time to distance from the sense wire. The tubes in the chambers with even numbers are tilted by 4°. The directions of protons and antiprotons are also shown.

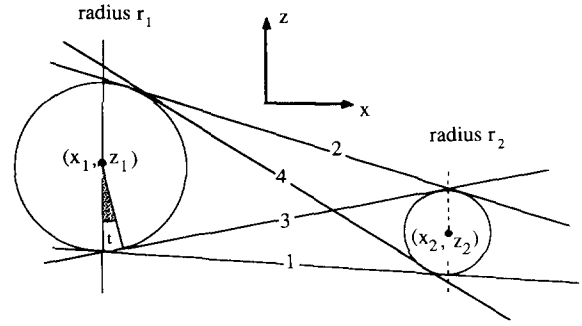

Fig. 14. Tracks which are tangential to two circles (hits). The number 1, 2, 3 and 4 and symbols correspond to the same in eq. (1)

The lines satisfy the following equations (see fig. 14 for the definition of variables):

$$\sin(t)(x_2 - x_1) - \cos(t)(z_2 - z_1) + (r_2 - r_1) = 0, \quad (1)$$

$$\sin(t)(x_2 - x_1) - \cos(t)(z_2 - z_1) - (r_2 - r_1) = 0, \quad (2)$$

$$\sin(t)(x_2 - x_1) - \cos(t)(z_2 - z_1) - (r_2 + r_1) = 0, \quad (3)$$

$$\sin(t)(x_2 - x_1) - \cos(t)(z_2 - z_1) + (r_2 + r_1) = 0. \quad (4)$$

After t is found from each equation, the slope ($\tan(t)$) and intercept are calculated for each line. Once the equation of a line is found, the line is projected to the next chamber (toward the interaction region) and the predicted position is compared with the measured position. If the difference is within a given limit, the hit is tagged to belonging to the line. A hit can be tagged by more than one line. The search continues until there are five good points or the search reaches chambers with appreciable magnetic field (first chamber). When the search is over, those tracks with more than four points are fitted with a straight line. If only one track is reconstructed and its χ^2/df is less than 2, then the track is accepted for further processing. If more than two tracks with χ^2/df less than 2 resulted from the four tangential lines, the track with the most points is selected. If the number of points is the same, then the line with best χ^2/df is chosen. Those hits belonging to good tracks are deleted from the data bank and not used further. This process is continued until all hits are tried.

Using the slope and intercept of the selected track, the approximate momentum of the track is calculated using the interaction vertex and the integrated magnetic field. Using this momentum, the track is swum through the magnetic field to the remaining chambers and the nearest hits within a given limit are selected. After all hits belonging to a track are found, the track is finally fitted with a second order polynomial.

After the horizontal position of a track is found, the hits in the slanted tubes along the track are collected. From the hits and known horizontal positions of the track, the corresponding vertical position of each hit in the slanted tubes is calculated. A linear fit is performed with the hits and the track with most hits (with good χ^2/df) is chosen. We found this procedure reconstructs tracks correctly with better than 95% efficiency.

6. Application for the Superconducting Super Collider

The concept of using straw tubes can be easily extended to a detector for the Superconducting Super Collider. As discussed earlier, there are several advantages of using tubes for a drift chamber. The chamber could be either a cylindrical central chamber or just a rectangular type tracking chamber [7].

The upper limit of the tube radius is set by the bunch spacing of the SSC. Since electrons produced from tracks of an interaction should have reached the sense wire before the next bunch arrives, the radius of the tubes should be about 1.5 mm if a fast gas with electron drift velocity 100 μm/ns is used. As shown previously, there are gases with drift velocity higher than 100 μm/ns within the small tubes under an operating voltage.

In this section we present some tests performed using 2 mm radius tubes. The tube wall is made of 0.025 mm thick mylar coated with 200–300 Å thick aluminum [8]. Several single straw tube prototype chambers were constructed with 25 μm diameter gold plated tungsten wire under 50 g tension. We were able to pressurize the chamber to 3 atm for a month without any problem. Pressurizing tubes not only keeps them round and stiff but also could result in a better resolution.

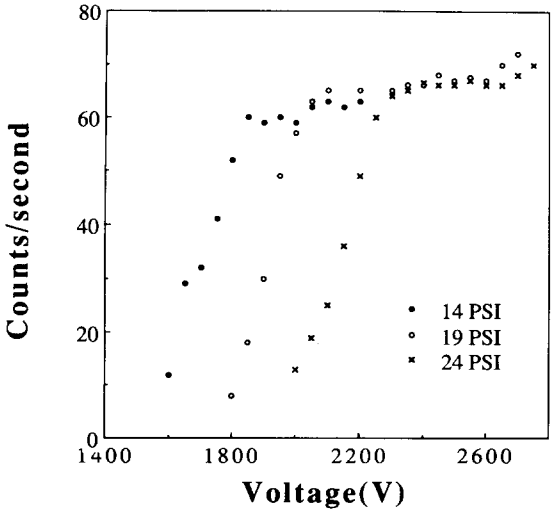

Fig. 15. Plateau curves obtained using small straw tubes (2 mm radius) filled with CH_4 under different pressures.

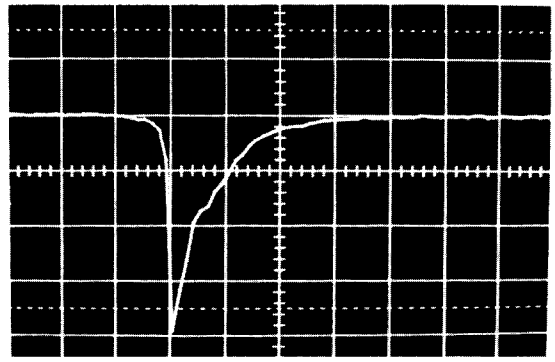

Fig. 16. The shape of the averaged signal using ^{90}Sr into a 50 Ω resistor. 1000 signals are averaged. HV = 2200 V, gas = methane. The vertical scale is 0.5 mV/div and the horizontal scale is 20 ns/div.

In fig. 15, plateau curves obtained with a ^{90}Sr source at several different pressures with pure methane are plotted. We observe a very nice plateau for all pressures. It is interesting that the knee of the plateau changes as a function of pressure. Fig. 16 shows an averaged signal using ^{90}Sr source. The gas mixture is pure methane at 1 atm and the high voltage is set at 2200 V. The peak is about 2 mV into a 50 Ω resistor. The signal rises to the maximum within 3 ns and falls to about 10% of the peak after 30 ns.

Using 4 mm diameter straw tubes, we have constructed a 60 channel, 2.7 m long prototype. It has eight layers of tubes. Some preliminary results are already reported [9]. The detailed construction and performance test will be reported in the near future.

References

[1] C. Broll et al., Nucl. Instr. and Meth. 206 (1983) 385;
P. Baringer et al., Nucl. Instr. and Meth. A254 (1987)542.
[2] T. Alexopoulos et al., Phys. Rev. Lett. 60 (1988) 1622;
S. Banerjee et al., Phys. Rev. Lett. 62 (1989) 12;
T. Alexopoulos et al., Phys. Rev. Lett. 64 (1990) 991.
[3] Stone Industrial Division, College Park 20704, MD, USA.
[4] C. Lindsey et al., Nucl. Instr. and Meth. A254 (1987) 212.
[5] M. Turala and J.C. Vermeulen, Nucl. Instr. and Meth. 205 (1983) 141.
[6] F. Sauli, CERN preprint 77-09;
B. Jean-Marie et al., Nucl. Instr. and Meth. 159 (1979) 213;
L. Christophorous et al., Nucl. Instr. and Meth. 163 (1979) 141;

T. Yamashita et al., KEK preprint 88–133;
there are some disagreements between published drift velocity measurements, for example, in CH_4.

[7] SSC subsystem proposals, submitted to SSC Lab, 1989, PC-024 (G. Hanson et al.), PC-035 (A.T. Goshaw et al.).

[8] The small radius tubes were wound by Precision Tubing, Wheeling, IL, USA.

[9] S.H. Oh et al., Proc. Int. Workshop on Solenoidal Detectors for the SSC, KEK, Japan, eds. F. Abe and R. Hasegawa (1990) p. 279.